

# Dimeric Surfactants: Spacer Chain Conformation and Specific Area at the Air/Water Interface

Haim Diamant and David Andelman\*

School of Physics and Astronomy, Raymond and Beverly Sackler Faculty of Exact Sciences,  
Tel Aviv University, Ramat Aviv, Tel Aviv 69978, Israel

Received January 3, 1994. In Final Form: May 30, 1994<sup>®</sup>

We present a theoretical explanation for experimental results obtained recently regarding dimeric surfactants. The nonmonotonic dependence of the specific area at the air/water interface on the spacer carbon number is accounted for. In addition, understanding the role of spacer carbon number at the air/water interface can elucidate the shapes of aggregates formed in the aqueous solution. The attractive and repulsive interactions of the surfactant molecules and the conformational entropy of the spacer chain are found to be dominant factors in determining this dependence. On the other hand, hydrophobic repulsion of the spacer from the water surface does not seem to play an important role, if any, contrary to what has been previously suggested.

## 1. Introduction

Interesting experiments have been recently performed on homologous series of *dimeric surfactants*.<sup>1-5</sup> These molecules are composed of ordinary surfactant monomers whose polar headgroups have been chemically linked in pairs by an alkanediyl chain ("spacer"). This linking leads to changes in the physical and chemical properties compared to those of the original monomers. In particular, we mention the solubility,<sup>1</sup> the critical micelle concentration,<sup>1,2</sup> the micellar ionization degree,<sup>2</sup> and interfacial properties at the air/water interface.<sup>5</sup> One of the most interesting phenomena observed is the influence of the spacer carbon number on the aggregate morphology:<sup>4</sup> monomers forming aggregates of a certain shape (*e.g.*, spherical micelles) self-assemble, after being linked into dimers, into aggregates of a different shape (spherical or cylindrical micelles, vesicles) depending on the spacer carbon number.

One of the main effects of introducing the spacer is to impose an additional geometrical constraint on the packing of surfactant molecules and, therefore, to influence their aggregate shape. The geometrical parameter determining the aggregate shape is the "packing parameter"<sup>6,7</sup>

$$p = v/l\Sigma \quad (1)$$

where  $v$  is the volume occupied by the hydrophobic moiety of the surfactant molecule,  $l$  its length, and  $\Sigma$  the area per molecule. While  $l$  is supposed to remain unchanged as the spacer carbon number is increased (as long as the spacer is not too long compared to the hydrophobic tails) and  $v$  is expected to have a slow monotonic increase,  $\Sigma$  is found in experiments to behave in a nonmonotonic manner.<sup>5</sup> It increases rapidly for short spacers (containing only several methylene groups), reaches a maximum for medium spacers (containing about 10 to 12 methylene groups for the dimers investigated in ref 5) and decreases

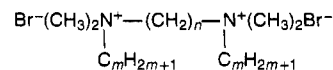
for even longer spacers (see Figure 1). Note that in the experiments<sup>5</sup>  $\Sigma$  is measured at the air/water interface but is assumed to be directly related to the area per molecule on the micelle.

In view of these observations, it seems that changes in the aggregate morphology for dimeric surfactants are mainly related to the influence of the spacer on the specific area  $\Sigma$ . For example, small  $\Sigma$  imposed by short spacers will lead to large packing parameter  $p$  and, thus, may account for the cylindrical micelles observed for such spacers. Similarly, close-to-maximum areas imposed by medium spacers may explain the spherical shapes. The decrease of  $\Sigma$  for longer spacers, together with the expected increase in  $v$  associated with such long chains, may account for structures such as vesicles or bilayer lamellae.

We focused, therefore, in the present work on a theoretical explanation for the dependence of the area  $\Sigma$  on the spacer carbon number. The various conformations available for the spacer chain comprise the main complication of the problem. On one hand, these conformations obviously play a crucial role since the spacer cannot be regarded as a rigid rod. On the other hand, the spacer chains are short (containing about 1 to 20 methylene groups), and one cannot implement the powerful results of polymer theory, applicable to very long chains. In order to overcome this problem, our treatment combines analytical formulation with computer simulations, allowing us to deal with *any* spacer carbon number. The outline of this work is as follows: We begin with a brief description of the relevant experimental system. Next, we present in section 3 a statistical-mechanical formulation resulting in an equation for the spacer carbon number for which the specific area is maximal. Finding this length requires statistical data about the conformations of the spacer chain. We acquire this information through computer simulations, which are discussed in section 4. The results of our analysis are presented in section 5. In section 6 we present a simplified approach, which helps to verify the validity of one of our major approximations. Finally, in section 7, concluding remarks are presented.

## 2. The Experimental System

The molecules studied in the experiments<sup>1-5</sup> are of the type



where  $m$  is the number of carbon atoms in each of the hydrophobic tails and  $n$  is the number of methylene groups in the spacer

<sup>®</sup> Abstract published in *Advance ACS Abstracts*, July 15, 1994.

(1) Devinski, F.; Lacko, I.; Tanweerul, I. *J. Colloid Interface Sci.* **1991**, *143*, 336-342.

(2) Zana, R.; Benraou, M.; Rueff, R. *Langmuir* **1991**, *7*, 1072-1075.

(3) Alami, E.; Levy, H.; Zana, R.; Skoulios, A. *Langmuir* **1993**, *9*, 940-944.

(4) Zana, R.; Talmon, Y. *Nature* **1993**, *362*, 228-229.

(5) Alami, E.; Beinert, G.; Marie, P.; Zana, R. *Langmuir* **1993**, *9*, 1465-1467.

(6) Israelachvili, J.; Mitchell, D. J.; Ninham, B. W. *J. Chem. Soc., Faraday Trans. 2* **1976**, *72*, 1525-1568.

(7) Israelachvili, J. *Intermolecular & Surface Forces*, 2nd ed.; Academic Press: London, 1991; Chapter 17.

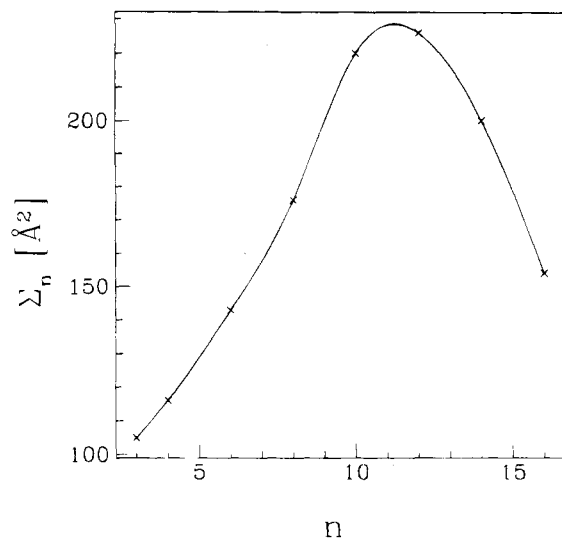


**Figure 1.** Area per surfactant molecule  $\Sigma$  at the air/water interface, as found in experiments, plotted against the number of methylene groups  $n$  in the spacer chain for  $n = 3, 4, 6, 8, 10, 12, 14,$  and  $16$  (reproduced from ref 5). The smooth curve connecting the experimental points is a fit used just as a guidance to the eye.

chain. The parameter  $n$  will be referred to, hereafter, as the *spacer length*. For  $m = 12$  this molecule may be considered as the dimer of two DTAB (dodecyltrimethylammonium bromide) monomers linked by a  $(\text{CH}_2)_n$  spacer.

The area per molecule of the monolayer at the water surface can be obtained from surface tension measurements. From the slope of the surface tension vs the log of the concentration, as one approaches the critical micelle concentration (cmc) from below, the surface-excess concentration  $\Gamma$  can be found. This last quantity is the number of molecules per unit area contributing to the concentration excess due to the interface

$$\Gamma = \int_0^{\infty} [c(z) - c_b] dz \quad (2)$$

where  $c(z)$  is the concentration profile as a function of the distance  $z$  from the air/water interface and  $c_b$  its value in the bulk ( $z \rightarrow \infty$ ). The surface-excess concentration can be found using the Gibbs equation in the dilute solution limit<sup>8</sup>

$$\Gamma = -\left(\frac{\partial \gamma}{\partial \mu}\right)_T \approx -\frac{1}{3k_B T} \left(\frac{\partial \gamma}{\partial \log c_b}\right)_T \quad (3)$$

where  $\gamma$  is the surface tension,  $\mu$  the chemical potential of the solute molecules,  $T$  the temperature, and  $k_B$  the Boltzmann constant. The prefactor  $1/3$  in eq 3 is due to the fact that the solute molecule dissolves into three ions—one divalent and two monovalent. Although there is some disagreement concerning this numerical prefactor,<sup>5</sup> it has no influence on the qualitative behavior as seen in experiments. For dilute surfactant solutions, the bulk concentration is much smaller than the concentration at the interface, so  $\Gamma$  is practically the same as the surface density  $\sigma$  of the monolayer. Hence, the area per molecule is simply given by

$$\Sigma = \frac{1}{\sigma} \approx \frac{1}{\Gamma} \quad (4)$$

The experimental values of  $\Sigma$  as a function of  $n$  were reported in ref 5 and are summarized in Figure 1. For  $n < 10$ , the specific area increases with increasing  $n$ , for  $n \sim 10-12$ , it reaches a maximum, and for  $n > 12$ , it decreases with increasing  $n$ .

### 3. The Model

Our aim in this section is to formulate the simplest model which would still explain the unique behavior of

dimeric surfactants at the air/water interface. Wishing to consider a minimal number of interactions, one can specify two factors which undoubtedly play an important role in this behavior, and therefore must be included: (i) the “surfactant nature” of the molecules, *i.e.*, their hydrophilic–hydrophobic interactions; (ii) the inherent characteristics of the spacer chain. These two factors alone will be shown to suffice for explaining the main features of the behavior at the interface.

In order to further simplify the model, we shall decouple the spacer contribution from the intermolecular interactions and treat it as an independent, internal degree of freedom of the molecule. This assumption can be justified for *soluble* monolayers, since the area per molecule at the interface corresponds to a *liquid expanded* state of the chains, and the configurational entropy is similar to that of free chains (or equivalently, a “melt” of chains).<sup>9</sup> The specific character of dimeric surfactants enters via geometrical constraints imposed by the interface and influencing the entropy due to the spacer chain configurations. In addition, average quantities such as the area per molecule are Boltzmann-weighted averaged and take into account intermolecular and intramolecular interactions.<sup>10</sup>

In accord with the experimental system described in section 2, we consider a surfactant monolayer at the air/water interface, whose total area is fixed and which is in thermodynamic equilibrium with a dilute surfactant solution of concentration  $c_b$ . The following formalism is valid only below the cmc, when the surfactant is solubilized as monomers in the solution. The free energy per unit area of the system,  $\gamma$ , can be written as

$$\gamma = \gamma_0 - \gamma_1 \quad (5)$$

where  $\gamma_0$  is the bare air/water surface tension and  $\gamma_1$  the reduction in the surface tension due to the surfactant. This reduction in free energy can be separated into two contributions

$$\gamma_1 = -(f_s + f_{ex}) \quad (6)$$

where  $f_s$  is the free energy per unit area of the surfactant molecules lying on the interface and  $f_{ex}$  the excess in free energy per unit area due to the increase in surfactant concentration below the interface. Within the mean-field approximation we can write (*e.g.*, ref 11)

$$f_{ex} = \int_0^{\infty} \left[ \frac{1}{2} B \left( \frac{\partial \phi}{\partial z} \right)^2 + \Omega(\phi) \right] dz \quad (7)$$

where  $B$  is the stiffness coefficient and  $\phi(z) = a^3 c(z)$  is the surfactant volume fraction ( $a$  being the molecular length). The function  $\Omega(\phi)$  may account for any local factors which are present in the bulk solution, such as short-range interactions between the monomers or the contact with the reservoir. Note, however, that eq 7 does not account for the long-range double-layer interaction, which depends on  $\partial \phi / \partial z$ . This interaction should indeed be present in the ionic solution of the experimental system discussed above

(9) Szleifer, I.; Ben-Shaul, A.; Gelbart, W. M. *J. Phys. Chem.* **1990**, *94*, 5081–5089.

(10) We do not consider interchain interactions between the spacer and other hydrocarbon chains in the monolayer. Although being present, these interactions are not essential for understanding the main phenomena.

(11) Safran, S. A. *Statistical Thermodynamics of Surfaces, Interfaces and Membranes*; *Frontiers in Physics*; Addison-Wesley: Reading, MA, 1994; Vol. 90, Chapter 2.

(8) Adamson, A. W. *Physical Chemistry of Surfaces*, 5th ed.; Wiley & Sons: New York, 1990; Chapter III.

but can be shown to have a minor effect.<sup>12</sup> Minimization of  $f_{\text{ex}}$  with respect to the profile  $\phi(z)$  leads, for any function  $\Omega(\phi)$ , to the expression

$$f_{\text{ex}} = B \int_0^{\infty} \left( \frac{\partial \phi}{\partial z} \right)^2 dz \quad (8)$$

For the dilute surfactant solutions used in the experiments, the surfactant volume fraction drops sharply from its value at the surface ( $\phi_s$ ) to its value in the bulk ( $\phi_b \ll \phi_s$ ) within a distance of the order of  $a$  from the interface. We may take eq 8, therefore, in the approximated form

$$f_{\text{ex}} \approx \frac{B}{a} (\phi_s - \phi_b)^2 \quad (9)$$

and rewrite eq 5 as

$$\gamma = \gamma_0 + f_s(\phi_s) + \frac{B}{a} (\phi_s - \phi_b)^2 \quad (10)$$

Minimizing it with respect to  $\phi_s$  yields

$$\frac{\partial f_s}{\partial \phi_s} + \frac{2B}{a} (\phi_s - \phi_b) = 0 \quad (11)$$

Utilizing again the fact that  $\phi_s \gg \phi_b$  and the relation  $\phi_s = a^2/\Sigma$ , we arrive at the equation for the area per molecule at equilibrium

$$\Sigma^3 \frac{\partial f_s}{\partial \Sigma} = 2a^3 B \quad (12)$$

Up until now, the treatment applies to dilute solutions of any soluble surfactant, without considering microscopic details of the surfactant molecule. The dimeric nature of the surfactant will appear only in the expression for  $f_s$ . The free energy per unit area of the dimers at the interface, leading to a reduction in the surface tension, may be written as

$$f_s = \frac{1}{\Sigma} [u_s - T s_{\text{tr}} + f_{\text{in}}] \quad (13)$$

where  $u_s$  is the intermolecular energy (per molecule) on the surface,  $s_{\text{tr}}$  the translational entropy per molecule, and  $f_{\text{in}}$  the *intramolecular* free energy arising from the configurations of the spacer chain and its intrachain interactions. The energy  $u_s$  may be taken to first approximation as a sum of two contributions<sup>6,7,13</sup>

$$u_s = \gamma_2 \Sigma + \frac{\alpha}{\Sigma} \quad (14)$$

The first term accounts for the attraction between the hydrophobic tails of the surfactant molecules ( $\gamma_2$  being the surface tension of hydrocarbon/water), while the second accounts for the repulsion between the headgroups. The two-dimensional translational entropy per molecule

(12) In a dilute solution such as the one we deal with, the electric field is unscreened and the counterion profile dominates. Neglecting the surfactant profile below the interface, the electric energy per unit area of such a double layer is just  $2k_B T/\Sigma$ , where  $\Sigma$  is the area per dimer at the air/water interface. This amounts, in the relevant experimental system, to about 4 dyn/cm. Taking more accurate estimates yields the same result. Since the reduction of surface tension due to the surfactant is about 30–40 dyn/cm, the relative unimportance of the double-layer interaction is established.

(13) The form of  $u_s$  as appears in eq 14 is appropriate for surfactant monolayers close to saturation. This, indeed, agrees with the experimental setup to which our model applies. In the very dilute limit, the surface tension of the monolayer should include a term linear in the surfactant concentration at the interface.

$s_{\text{tr}}$  can be written as

$$s_{\text{tr}} = \log \frac{\Sigma}{a^2} + \left(1 - \frac{\Sigma}{a^2}\right) \log \left(1 - \frac{a^2}{\Sigma}\right) \quad (15)$$

where we set hereafter the Boltzmann constant  $k_B \equiv 1$ . Substituting (14) and (15) in eq 13 and then in eq 12 gives

$$-\Sigma \left[ f_{\text{in}} - \Sigma \frac{\partial f_{\text{in}}}{\partial \Sigma} - T \log \left( \frac{\Sigma}{a^2} - 1 \right) \right] = 2(a^3 B + \alpha) \quad (16)$$

The main complication in the case of dimeric surfactants is that the spacer chain cannot be regarded as a rigid rod of fixed length but rather takes various spatial configurations, which influence the value of  $\Sigma$ . The parameter of interest in our problem is the *end-to-end* distance  $r$  of the chain (*i.e.*, the distance between the two headgroups of the dimer which are restricted to lie on the air/water interface), since it constitutes the geometrical constraint on the arrangement of the dimers at the interface. Spacer chains of different lengths, *i.e.*, containing a different number of groups  $n$ , have different sets of configurations, leading to different distributions of the end-to-end distance  $r$ .

The distributions of  $r$  for short chains ( $n$  being in the range of 1 to 20) are generated numerically as discussed in section 4. They are quite complicated but still characterized by a single peak. In order to make the analysis easier, we replace the actual distribution by a Gaussian one with the same mean  $E_n$  and variance  $V_n$ . We would like to emphasize that this fit *does not* imply that our chains are Gaussian chains themselves. The fit is used just to facilitate our analysis, since the distribution can be well parametrized by its first two moments.

The number of configurations giving rise to a distance in a small range  $\Delta r$  around  $r$  is given then, up to a normalization factor, by

$$g_n \Delta r \propto \frac{\Delta r G_n}{(2\pi V_n)^{1/2}} \exp \left[ \frac{-(r - E_n)^2}{2V_n} \right] \quad (17)$$

where  $G_n$  is the total number of configurations of the chain. We may, therefore, write the intramolecular free energy of the dimer due to the spacer as

$$-f_{\text{in}}/T = \log(g_n \Delta r) \approx C_n - (r - E_n)^2/(2V_n) \\ C_n = \log[G_n (2\pi V_n)^{-1/2} \Delta r] + \text{const} \quad (18)$$

Note that the intrachain free energy  $f_{\text{in}}$  includes a Boltzmann-weighted summation over the chain configurations taking into account intrachain interactions. Substituting (18) in eq 16 yields

$$T\Sigma \left[ \log \left( \frac{\Sigma}{a^2} - 1 \right) + C_n - \frac{(r - E_n)^2}{2V_n} + \Sigma \frac{r - E_n}{V_n} \frac{dr}{d\Sigma} \right] = 2(a^3 B + \alpha) \quad (19)$$

Seeking an equation for the area per dimer  $\Sigma$ , we need to know its dependence on the distance  $r$  between the headgroups. The exact dependence is complicated, since  $\Sigma$  affects (*e.g.*, through  $u_s$ ) the probabilities of configurations available for the spacer. However, one can justify two heuristic arguments: (i) the area  $\Sigma$  is a monotonic increasing function of  $r$  (we expect the molecular area to grow when the two headgroups get further apart); (ii) this dependence must be weaker than quadratic, since  $r$  is only one of the two significant lengths on the surface (the

other being the distance between nearest neighboring headgroups *not* linked by a spacer). Consider as an example the case of a long-range two-dimensional positional order of the dimers on the surface. The area per dimer would be  $R(r + R)$ , where  $R$  is the distance between unlinked nearest neighboring heads. In view of these arguments we shall assume a linear dependence between  $\Sigma$  and  $r$

$$r = m_0 + m_1 \Sigma \quad (20)$$

Then, eq 19 becomes

$$T\Sigma \left[ \log\left(\frac{\Sigma}{a^2} - 1\right) + C_n + \frac{(m_1 \Sigma)^2 - (m_0 - E_n)^2}{2V_n} \right] = 2(a^3 B + \alpha) \quad (21)$$

If we knew all the relevant constants, eq 21 would enable us to find the equilibrium  $\Sigma = \Sigma_n$  for various spacer lengths  $n$ . However, since the values of  $B$ ,  $a$ , and  $\alpha$  can only be roughly estimated, we will concentrate mainly upon finding the spacer length  $n^*$  corresponding to the *maximal* specific area, in accord with Figure 1. We regard  $n$  as a continuous variable and differentiate eq 21 with respect to it while keeping  $\Sigma$  constant. This yields an equation for  $n^*$  which is *independent* of the *unknown* constants ( $B$ ,  $a$ ,  $\alpha$ )

$$\frac{dC_n}{dn} + \frac{(m_0 - E_n)}{V_n} \frac{dE_n}{dn} - \frac{(m_1 \Sigma^*)^2 - (m_0 - E_n)^2}{2V_n^2} \frac{dV_n}{dn} = 0 \quad (22)$$

where  $\Sigma^* = \Sigma(n^*)$  is the maximal specific area.

In the last differentiation it was implicitly assumed that the compact molecular length  $a$  and the energy parameter  $\alpha$  (eq 14) do not change appreciably when the spacer length is changed. This assumption is valid for  $a$  when the spacer is long enough, so that the chain flexibility allows the "hard core" area  $a^2$  to be about twice that of the monomeric surfactant. For spacer lengths of more than eight to ten groups, the spacer is flexible enough to allow configurations of very small end-to-end distance. Hence, it is indeed reasonable to assume that  $a$  is a constant for  $n$  above these values. As for  $\alpha$ , this parameter is characteristic of the repulsive interaction among the headgroups and should not depend strongly on the spacer length. Equation 22 is the key equation of this formulation. It should enable us to find the spacer length  $n^*$  corresponding to the maximal specific area.

#### 4. Simulations of the Spacer Chain

In order to use eq 22 and find  $n^*$ , we have to determine the functions  $E_n$  and  $V_n$ . In other words, we need statistical information about the configurations of the spacer chain for various spacer lengths,  $n$ , and about the distributions of the end-to-end distance  $r$  derived from them. The information can be obtained from the widely-used model for hydrocarbon chains, namely the *rotational-isomeric* model.<sup>14-17</sup> According to this model, the length of C—C bonds in the chain and the angles between them are fixed.

(14) Flory, P. J. *Statistical Mechanics of Chain Molecules*; Wiley & Sons: New York, 1969; Chapters III and V.

(15) Scott, R. A.; Scheraga, H. A. *J. Chem. Phys.* **1964**, *42*, 2209–2215.

(16) Scott, R. A.; Scheraga, H. A. *J. Chem. Phys.* **1965**, *44*, 3054–3069.

(17) Abe, A.; Jernigan, R. L.; Flory, P. J. *J. Am. Chem. Soc.* **1966**, *88*, 631–639.

Each bond may take one of three rotational states (*trans*, *gauche*<sup>+</sup>, and *gauche*<sup>-</sup>).

Distributions of the end-to-end distance corresponding to the rotational-isomeric model are analytically derived for long chains (polymers).<sup>14</sup> However, they give a monotonic increase of  $\Sigma$  as a function of  $n$ , in contrast to the experimental observation seen for relatively short chains,  $n \sim 1-20$  (see Figure 1). More specifically, the analysis for long chains predicts a linear dependence of the variance  $V_n$  on  $n$ . As will be shown below, a faster increase of  $V_n$  is needed in order to obtain the nonmonotonic behavior of  $\Sigma$  where  $n$  is increased.

Therefore, we have to rely on computer simulations to generate *short* chain configurations according to the rotational-isomeric model. For spacer chains, additional geometrical constraints should be taken into account. First, the entire chain is restricted to the half-space above the air/water interface, because of the high hydrophobic energy associated with immersing hydrocarbon groups in water. Second, the two ends of the chain should be "pinned" to the interface (we took one end exactly on the interface while allowing the other to get as far as 1 Å from the interface). The spacer is treated as an isolated chain, neglecting its excluded-volume interactions with the hydrophobic tails or with chains of other molecules. In this sense, the simulations are actually of *bola* surfactants,<sup>18</sup> which are surfactants consisting of two headgroups linked by a single hydrophobic chain ( $m = 0$  in our notation), rather than dimeric surfactants. For simplicity, we took the terminal bonds to be C—C bonds instead of the actual C—N<sup>+</sup> ones. The distributions of the end-to-end distance were obtained by computer simulations generating 10<sup>6</sup> chain configurations complying with all the above conditions.

In addition to the usual rotational-isomeric model, two other modified models were studied. The first includes attractive interactions between nonbonded groups along the chain. The original derivation of the conformational states in the rotational-isomeric model itself<sup>14-17</sup> involved, in fact, the same attractive interactions but only between groups which are three or four bonds apart. Therefore, the first modification we introduce is merely to consider attractive interactions between nonbonded pairs of groups which are five or more bonds apart. As opposed to chains which can take any configuration in space, the restriction to half-space and the "pinning" of the ends to the interface cause the attractive interactions from all the pairs of groups to add up in one direction, leading to a shorter end-to-end distance. In view of this unidirectional preference, these interactions turn out to be quite significant. For the intergroup pair potential we used a "6-exp" Buckingham potential<sup>14-17</sup>

$$U_{ij} = c_1 \exp(-c_2 r_{ij}) - c_3 / r_{ij}^6 \quad (23)$$

where the first term accounts for the hard core repulsion and the second for the van der Waals attraction,  $r_{ij}$  is the distance between groups  $i$  and  $j$  and  $c_1$ ,  $c_2$ , and  $c_3$  are constants of the values  $6.32 \times 10^{-15}$  J,  $4.59 \text{ \AA}^{-1}$ , and  $2.52 \times 10^{-18} \text{ J \AA}^6$ , respectively.<sup>17</sup> Only interactions between carbon atoms are considered, neglecting those between hydrogen atoms and between carbons and hydrogens.

Another modified model we employed adds to the rotational-isomeric model a hydrophobic repulsion of the chain groups from the interface. Such an effect was suggested before<sup>1,5,19,20</sup> as being responsible for phenomena

(18) Nagarajan, R. *Chem. Eng. Commun.* **1987**, *55*, 251–273.

(19) Verrall, R. E.; Milioto, S.; Zana, R. *J. Phys. Chem.* **1988**, *92*, 3939–3943.

**Table 1. The Mean and Variance of the End-to-End Distance Obtained from Computer Simulations of Spacer Chains of Length  $n = 1$  to 20<sup>a</sup>**

$n$	RI model		NA model		HR model	
	$E_n$	$V_n$	$E_n$	$V_n$	$E_n$	$V_n$
1	1.66	0	1.66	0	1.66	0
2	2.27	0.0715	2.27	0.0715	2.27	0.0715
3	3.02	0.0655	3.02	0.0656	3.02	0.0671
4	3.56	0.119	3.56	0.119	3.52	0.111
5	4.18	0.233	4.18	0.233	3.83	0.321
6	4.63	0.291	4.62	0.296	4.07	0.28
7	5.17	0.514	5.13	0.531	4.40	0.39
8	5.55	0.677	5.48	0.724	4.76	0.60
9	5.99	1.05	5.87	1.16	5.07	0.83
10	6.32	1.36	6.15	1.56	5.42	1.15
11	6.70	1.89	6.46	2.24	5.71	1.45
12	6.99	2.36	6.68	2.87	6.05	1.89
13	7.31	3.07	7.00	3.39	6.32	2.3
14	7.57	3.66	7.17	4.25	6.65	2.9
15	7.87	4.5	7.38	5.1	6.90	3.3
16	8.12	5.2	7.51	6.1	7.2	4.0
17	8.37	6.1	7.72	6.9	7.5	4.6
18	8.61	7.0	7.86	7.9	7.8	5.4
20	9.08	8.8	8.12	9.9	8.3	6.9

<sup>a</sup> RI, NA, and HR stand respectively for the three models used: rotational-isomeric, nonbonded attraction, and hydrophobic repulsion. The length of a single C—C bond,  $L = 1.526 \text{ \AA}$ , is taken as a unit length. For  $n = 1$ , the chain has only one configuration, so the end-to-end distance is fixed and the variance vanishes. All the listed values are given within an error of  $\pm 1$  in their last digit.

observed for long spacers, including the decrease in  $\Sigma_n$  as a function of  $n$ . A repulsive energy of  $4.9 \times 10^{-21} \text{ J}$  (corresponding to  $0.7 \text{ kcal mol}^{-1}$ ) was assigned to each group lying closer than  $2 \text{ \AA}$  to the air/water interface. The three models used in simulating the spacer chain will be referred to, hereafter, as RI (plain rotational-isomeric model), NA (nonbonded attraction), and HR (hydrophobic repulsion).

The moments of the distribution,  $E_n$  and  $V_n$ , obtained from the simulation of chains of various lengths using these three models, are listed in Table 1 (the length of one C—C bond in the chain,  $L = 1.526 \text{ \AA}$ , is taken to be a unit length). The dependence of  $E_n$  and  $V_n$  on the chain size  $n$  is also shown in Figure 2. Since it is more convenient to interpolate between the discrete values of  $n$ , we fit  $E_n$  and  $V_n$  with simple polynomials

$$E_n = k_2 n^2 + k_1 n + k_0$$

$$V_n = l_3 n^3 + l_0 \quad (24)$$

It should be stressed that  $k_i$  and  $l_i$  are not additional parameters entering the formalism but merely fitting coefficients introduced for mathematical convenience. The fitting coefficients obtained for the three models are listed in Table 2 and are used for evaluating  $n^*$  in eq 22.

Using the fact that

$$\frac{dC_n}{dn} = \frac{1}{G_n} \frac{dG_n}{dn} - \frac{1}{2V_n} \frac{dV_n}{dn} \quad (25)$$

the last quantity needed for eq 22 is the total number of configurations of the chain,  $G_n$ . According to the rotational-isomeric model, this number can be estimated roughly as  $3^{n-1}$ , or more generally

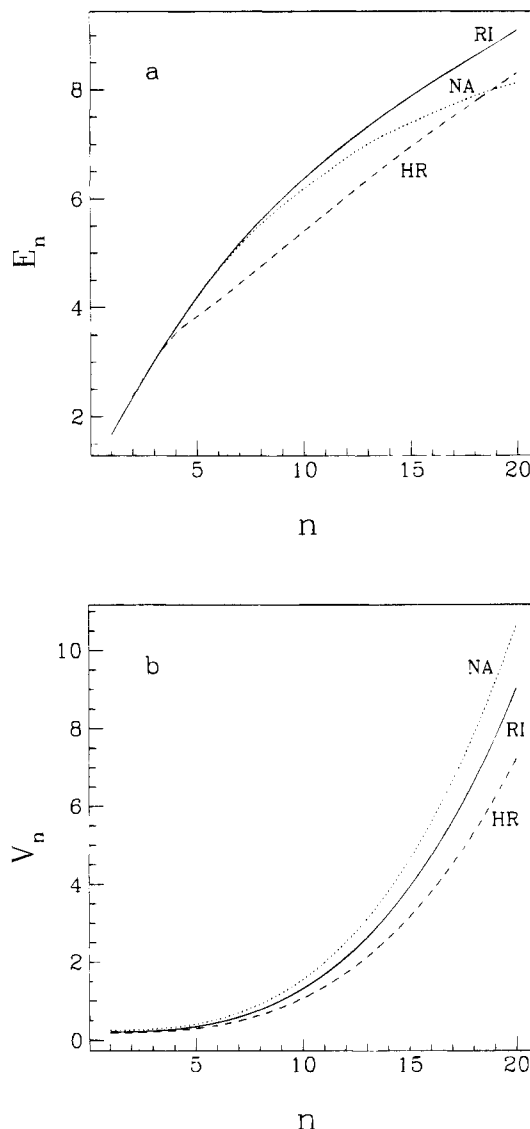


**Figure 2.** Mean  $E_n$  (a) and variance  $V_n$  (b) of the end-to-end distance, obtained from computer simulations, plotted against the spacer length  $n$ . The solid, dotted, and dashed curves are obtained by using the RI (rotational-isomeric), NA (nonbonded attraction), and HR (hydrophobic repulsion) models, respectively. The length of a single bond,  $L = 1.526 \text{ \AA}$ , is taken as a unit length.

**Table 2. Numerical Values (to Two Significant Digits) for the Fitting Coefficients Defined in eq 24<sup>a</sup>**

coefficient	RI model	NA model	HR model
$k_0$	1.1	1.1	1.5
$k_1$	0.65	0.66	0.45
$k_2$	-0.013	-0.016	-0.0058
$l_0$	0.21	0.25	0.19
$l_3$	0.0011	0.0013	0.00088

<sup>a</sup> RI, NA, and HR stand, respectively, for the three models: rotational-isomeric, nonbonded attraction, and hydrophobic repulsion. The length of a single C—C bond,  $L = 1.526 \text{ \AA}$ , is taken as a unit length.

$$G_n \approx \exp[q(n-1)] \quad (26)$$

where the value of  $q$  is about  $\log 3$ .

### 5. The Spacer Length of Maximal Specific Area

The aim of the preceding section was to obtain statistical information, allowing us to implement eq 22 and find the spacer chain length,  $n^*$ , corresponding to the maximal

**Table 3. Expressions and Approximate Values for the Coefficients of eq 27<sup>a</sup>**

coeff	exact expression	RI model	NA model	HR model
$\beta_0$	$2l_0[ql_0 - k_1(k_0 - m_0)]$	-0.56	-0.65	-0.48
$\beta_1$	$-2l_0[k_1^2 + 2k_2(k_0 - m_0)]$	-0.15	-0.18	-0.062
$\beta_2$	$3\{l_3[(k_0 - m_0)^2 - (m_1\Sigma^*)^2] - l_0(l_3 + 2k_1k_2)\}$	-0.20	-0.23	-0.21
$\beta_3$	$4[k_1l_3(k_0 - m_0) + l_0(ql_3 - k_2^2)]$	$7.7 \times 10^{-3}$	$9.4 \times 10^{-3}$	$5.9 \times 10^{-3}$
$\beta_4$	$l_3[k_1^2 + 2k_2(k_0 - m_0)]$	$4.0 \times 10^{-4}$	$4.7 \times 10^{-4}$	$1.4 \times 10^{-4}$
$\beta_5$	$-3l_3^2$	$-3.6 \times 10^{-6}$	$-5.1 \times 10^{-6}$	$-2.3 \times 10^{-6}$
$\beta_6$	$l_3(2ql_3 - k_2^2)$	$2.5 \times 10^{-6}$	$3.4 \times 10^{-6}$	$1.7 \times 10^{-6}$

<sup>a</sup> Substituting these coefficients in eq 27 yields  $n^* = 12.6, 12.2,$  and  $15.5$  for the RI, NA, and HR models, respectively. For all three models we take  $q = \log 3$  and  $\Sigma^* = 200 \text{ \AA}^2$ . The parameters fitted from experiments are  $m_0 = -1.3, m_1 = 0.097$  for the RI and NA models and  $m_0 = -1.8, m_1 = 0.11$  for the HR model. For the values of  $l_0, l_3, k_0, k_1,$  and  $k_3,$  see Table 2.

specific area,  $\Sigma^*$ . This is achieved and summarized in eqs 24 and 26 and Table 2. Substituting eqs 24 and 26 into eq 22 results in a 6th-order equation for  $n^*$

$$\sum_{i=0}^6 \beta_i (n^*)^i = 0 \quad (27)$$

In Table 3, we give explicit expressions for the  $\beta_i$  coefficients in terms of the parameters defined earlier.

The approximate linear dependence between  $r$  and  $\Sigma$  (eq 20) is best fitted from the first two or three points in the experimental data, corresponding to the specific area  $\Sigma$  which were measured for the shortest spacers. For such spacers the chain is rigid, the distribution of  $r$  is narrow, and  $r$  can be practically taken as  $E_n$  (see Table 1). The first three points taken from ref 5 do depend linearly on  $E_n$  for the RI and NA models, and give:  $m_0 = -1.3, m_1 = 0.097$  (recalling that all lengths are rescaled by the bond length  $L = 1.526 \text{ \AA}$ ). For the HR model, we get from the first two points:  $m_0 = -1.8, m_1 = 0.11$ .

Taking  $q = \log 3, \Sigma^* = 200 \text{ \AA}^2 \approx 86L^2$ , and the coefficients for the RI model from Table 2, eq 27 has a single positive solution:  $n^* \sim 12-13$  (see Table 3 for more details). This result is in accord with the experimental result  $n^* \sim 10-12$ . Since for very short and rigid spacers (say,  $n \sim 1-3$ ),  $r$  and  $\Sigma$  must increase with  $n$ , this extremum is indeed a maximum. Repeating the same procedure for the NA model gives similar results ( $n^* \sim 12-13$ ), while the HR model gives a higher value of about  $n^* \sim 15-16$ .

The most questionable of the values substituted above are those assigned to  $q$  and  $\Sigma^*$ , but varying these parameters in the range of  $q \sim \log 2 - \log 4, \Sigma^* \sim 150-250 \text{ \AA}^2$  still gives reasonable solutions of eq 27 in the range of  $n^* \sim 8-17$ . We also note that there is a disagreement, already mentioned in section 2, concerning the prefactor in the Gibbs equation (3) as applied to the relevant experimental system.<sup>5</sup> This disagreement results in two different sets of values for specific areas found in the experiments. The above results were obtained using the first set of values in ref 5. Taking the other set leads, nevertheless, to similar results.

## 6. Simplified Monolayer: No Exchange with the Bulk

In the preceding section the spacer length corresponds to the maximal specific area was calculated. Apart from this maximum, one may be also interested in obtaining, at least qualitatively, the whole dependence of the specific area on the spacer length. To this end we consider a simplified model of a monolayer containing a fixed number of dimers. The average specific area for a given  $n$ ,  $\langle \Sigma_n \rangle$ , is calculated by summing over chain configurations with a weight  $w(\Sigma)$

$$\langle \Sigma_n \rangle = \left( \sum_{\text{config}} w(\Sigma) \Sigma \right) / \sum_{\text{config}} w(\Sigma) \quad (28)$$

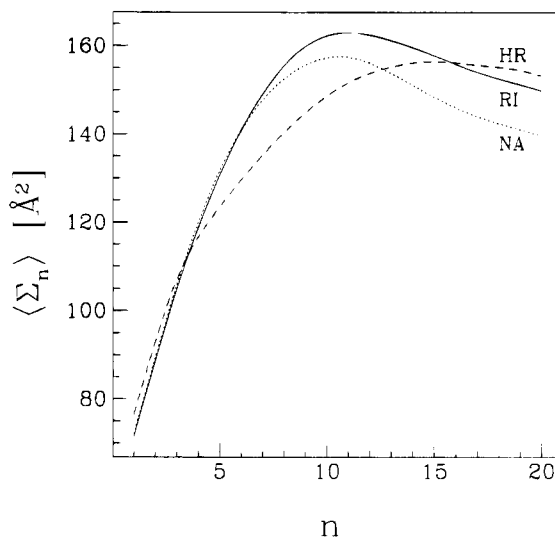


**Figure 3.** Boltzmann-weighted specific area ( $\Sigma_n$ ) plotted against the spacer length  $n$ . The solid, dotted, and dashed curves represent the RI, NA, and HR models, respectively. The unit length is taken as  $L = 1.526 \text{ \AA}$ .

where the weight  $w(\Sigma)$  is

$$w(\Sigma) = \exp[-u_s/T + s_{tr} - f_{in}/T] \quad (29)$$

The translational entropy as a function of  $\Sigma$  is taken from eq 15. When  $\Sigma \gg a^2$ ,  $\exp s_{tr} \propto \Sigma$ . It should be noted that here we do not fit the actual distribution of configurations to a Gaussian as was done in section 3. Rather, the factor  $\exp(-f_{in}/T)$  is just  $g_n[r(\Sigma)]$  and is taken directly from the simulated distributions. The expression for the intermolecular energy  $u_s$  is given by eq 14 and may be rewritten conveniently<sup>7</sup> as

$$u_s = \frac{\gamma_2}{\Sigma} (\Sigma - \Sigma_0)^2 + \text{const} \quad (30)$$

where  $\Sigma_0 = (\alpha/\gamma_2)^{1/2}$  is an "optimal specific area" resulting from the interplay between the intermolecular attractive and repulsive interactions. We took  $\gamma_2$  (the surface tension of hydrocarbon/water) to be  $50 \text{ mN m}^{-1}$  and  $\Sigma_0/2$  to be the optimal area of DTAB monomers, that is about  $55 \text{ \AA}^2$ . For each given spacer length  $n$ , averaging  $\Sigma$  according to eq 28 with the weight  $w(\Sigma)$  of eq 29 gives us  $\langle \Sigma_n \rangle$ . The resulting dependence of  $\langle \Sigma_n \rangle$  on  $n$  for the three models, RI, NA, and HR, is plotted in Figure 3.

We remark that the simplified model presented in this section does not fully describe the real experimental system. In contrast to experiments, it contains a fixed number of molecules at the surface and does not allow for exchange of surfactant molecules with the bulk solution. These factors are probably important in determining the actual numerical values of the specific area, but it is likely that they are not as dominant in determining its qualita-

tive dependence on the spacer length. As can be seen from Figure 3, the results of the simplified model turn out to qualitatively agree with experiments: the graphs show the expected nonmonotonic behavior of  $\Sigma$ , and the locations of maxima are generally consistent with those obtained in section 5 using the more detailed analysis.

The simplified model has, nevertheless, a 2-fold advantage over the detailed treatment of the preceding section. First, it provides a closer look at the difference between the three models used in the simulations, as will be discussed below. Second, it allows us to bypass one of the major approximations employed in our analysis. Whereas in the previous analysis our statistics were fitted to a Gaussian distribution, here the actual distribution of the real end-to-end distance is obtained directly from the computer simulations and is used for calculating  $\langle \Sigma_n \rangle$ .

## 7. Concluding Remarks

In this paper, we propose a theoretical explanation for the experimentally observed dependence of the specific area  $\Sigma$  of dimeric surfactants at the air/water interface on the spacer length  $n$ . This dependence is of importance for understanding the influence of the spacer length on the morphology of aggregates formed in the solution. Our analysis results in an equation for the spacer length corresponding to the maximal specific area. Substituting in this equation statistical data obtained from computer simulations of spacer chains, we get a solution which is in good quantitative agreement with the experiments.

In addition, the model presented here gives some insight on the dominant factors determining the dependence of the specific area on spacer length. Considering only geometrical packing constraints, longer spacers should lead basically to longer end-to-end distances  $E_n$  (Figure 2a), and hence to larger specific areas  $\Sigma_n$ . However, when the spacer becomes longer and tries to impose a specific area larger than the optimal one,  $\Sigma_0$ , the interaction among the surfactant monomers becomes attractive and tends to reduce this area (eq 30). The other important effect associated with longer spacers is the increase in chain flexibility. This is reflected by the fast increase of the variance of the end-to-end distance  $V_n$  with increasing spacer length (Figure 2b). The more flexible the spacer is, the more effective the attractive interaction becomes. The interaction among the surfactant monomers  $u_s$  and the conformational entropy of the spacers  $-f_{in}/T$  act, therefore, in a combined way to reduce  $\Sigma_n$ . The specific area reaches a maximum and then decreases as the spacer length is further increased.

This general description clarifies the difference between the three models presented in section 4 for generating configurations of spacer chains. The intrachain attraction included in the NA model should encourage the appearance of a maximum in  $\Sigma_n$ , since it shortens the end-to-end distance and becomes stronger as more methylene groups are added to the spacer chain. Moreover, the NA model shows the fastest increase in spacer flexibility (Figure 2b). Indeed, looking at the graphs obtained in section 6 using the simplified model (Figure 3), the NA model is found to show the sharpest maximum.

The HR model introduces hydrophobic repulsion of the spacer from the air/water interface. Its agreement with the experimental findings is poorer than that of the other two models. This result is obtained from both the detailed analysis (section 5) and the simplified one (section 6 and Figure 3), and is due, probably, to the slower increase in chain flexibility obtained for the HR model (Figure 2b). For a given spacer length, the hydrophobic repulsion leads, as expected, to shorter end-to-end distances (compare the curves in Figure 2a) and, hence, to smaller specific areas.

However, interactions such as the hydrophobic repulsion, which reduce the specific area, do not explain the nonmonotonicity of  $\Sigma_n$  when the spacer becomes longer. In order to overcome the basic tendency of the specific area to increase for longer spacers, an effect should get stronger as the spacer length is increased. Hydrophobic repulsion from the interface does not have this property, while attraction among the monomers, flexibility of the spacers, and intrachain attraction do.

In conclusion, it was found that the dependence of the specific area of dimers at the air/water interface on the spacer is dominated by the interplay of three factors. The first is merely the geometrical effect of lengthening the spacer, which in turn tends to increase the specific area. The second is the interaction among the surfactant monomers, which tends to decrease the specific area after the spacer has reached a certain length. The third is the conformational entropy of the spacer chain, which increases rapidly with spacer length and enhances the effect of the second factor. Introducing intrachain attraction between nonbonded groups along the spacer chain leads to an improved description of this dependence (a sharper maximum). Hydrophobic repulsion of the spacer chain from the air/water interface does not seem to play an important role, if any. Other interactions which must be present in the monolayer were ignored by our analysis. Among these we mention van der Waals attraction and excluded-volume repulsion between the spacer and other chains—the hydrophobic tails of the same dimer or chains belonging to other dimers. The agreement of our results with the experimental findings suggests, however, that these interactions are probably not dominant in determining the qualitative dependence of the specific area on the spacer length.

The treatment of the problem of dimeric surfactants presented in this work has been applied only to the case of the  $[\text{N}^+(\text{CH}_3)_2\text{C}_{12}\text{H}_{25}\text{Br}^-]_2(\text{CH}_2)_n$  dimers. It should be valid, of course, for any soluble dimeric surfactant, but more experiments are needed in order to verify the general nature of our predictions. Moreover, since the hydrophobic tails of the dimer do not enter explicitly in the analysis, this treatment may be applicable also to bola amphiphiles.<sup>18,20</sup> It should be borne in mind, however, that for bola amphiphiles the changes in specific area are not sufficient for explaining changes in aggregate morphology. Unlike the case of dimeric surfactants, the length of the hydrophobic moiety (referred to as  $l$  in the Introduction) depends, for bola surfactants, on the length of the connecting chain.

Finally, our analysis still uses some fitting to experimental data ( $m_0, m_1$ ) in order to determine the dependence between the specific area of the dimer and the distance between its headgroups. A theoretical estimate of this dependence will undoubtedly improve our description. Other possible directions will be to calculate the dependence of the cmc and the micellar shape on the spacer length. This, hopefully, will enable a fuller theoretical treatment of dimeric surfactants.

**Acknowledgment.** We thank R. Zana for introducing us to the subject of dimeric surfactants and for many useful comments and suggestions. We also benefited from discussions with A. Ben-Shaul, S. Safran, I. Szleifer, Y. Talmon, and Z.-G. Wang. Partial support from the German-Israel Foundation (G.I.F.) under Grant No. I-0197 and the Israel Academy of Sciences and Humanities is gratefully acknowledged.